IOP Publishing Superconductor Science and Technology
Supercond. Sci. Technol. **20** (2007) 728–735 doi:10.1088/0953-2048/20/8/002

Magnetic, transport and high-pressure properties of a $W_7Re_{13}B$ superconducting compound

B Andrzejewski[1,2,4], A Kowalczyk[1], A Jezierski[1] and M R Lees[3]

[1] Institute of Molecular Physics PAS, Smoluchowskiego 17, PL-60179 Poznań, Poland
[2] Laboratoire CRISMAT, UMR 6508 CNRS-ENSICAEN, 6, Boulevard du Maréchal Juin, F-14050 Caen Cedex, France
[3] Physics Department, University of Warwick, Coventry CV4 7AL, UK

E-mail: and@ifmpan.poznan.pl

Received 18 April 2007
Published 12 June 2007
Online at stacks.iop.org/SUST/20/728

Abstract
In this report we present experimental and theoretical investigations of the properties of the recently discovered $W_7Re_{13}B$ superconductor. This compound is synthesized by means of inductive melting and contains a pure phase with a sharp superconducting transition at $T_c = 7.22$ K. The superconductor exhibits type-II behaviour with reversible magnetic properties in a large part of the H–T diagram. The irreversibility line with the irreversibility field $\mu_0 H_{irr}(0)$ equal to 2 T is well separated from the upper critical field. The values of lower $\mu_0 H_{c1}(0)$ and upper $\mu_0 H_{c2}(0)$ critical fields are equal to 8.8 mT and 11.8 T, respectively. These values correspond to penetration depth λ, coherence length ξ and Ginzburg–Landau coefficient κ equal to 2675 Å, 52 Å and 51, respectively. The critical current density J_c is low and equal to 4.9 kA cm^{-2} at zero magnetic field and at 2 K. The effect of pressure on superconducting properties is almost negligible, probably due to the low compressibility of this compound. The pressure coefficient dT_c/dP is negative and equal to -0.037 K GPa^{-1}. The XPS spectrum and numerical calculations confirm that the main contributions to the density of states at the Fermi level come from W(5d) and Re(5d) states.

(Some figures in this article are in colour only in the electronic version)

1. Introduction

The discovery of high-T_c superconductivity in MgB_2 has renewed interest in intermetallic superconductors that contain low mass elements. The strong electron–phonon interaction and high frequency vibrations of lighter elements in these materials promote enhanced critical temperatures. From this point of view the best candidates for superconductors should be AlB_2-type diborides. Unfortunately, among the systems of AB_2 type with alkali metal A = Li, Be or Al none of them exhibits superconductivity. Only recently, the superconductivity at a temperature below 0.72 K was reported in $BeB_{2.75}$ characterized by a very complex and rare structure [1]. Diborides, isostructural to MgB_2 and formed with transition metals like Ti, Zr, Hf, V, Nb, Ta, Cr or Mo, were reported by Leyarovska [2]. In these systems, superconductivity was discovered by Cooper in NbB_2 with $T_c = 3.87$ K, in $Zr_{0.13}Mo_{0.87}B_2$ with T_c above 11 K [3] and by Kaczorowski in TaB_2 with relatively high critical temperature equal to 9.5 K [4]. It is evident that superconducting properties of these compounds are strongly influenced by exact composition [5]. For example Leyarovska [2] has found superconductivity in a NbB_2 system only, with lowered critical temperature equal to $T_c = 0.62$ K. On the other hand, Gasparov has not confirmed superconductivity in TaB_2 and NbB_2 systems at all but he found a superconducting phase ZrB_2 with $T_c = 5.5$ K [6]. There are also known superconducting ReB systems, for example Re_2B with $T_c = 2.8$ K [7]. Strukova

[4] Author to whom any correspondence should be addressed.

et al have reported superconductivity in a Re_3B compound with $T_c = 4.7$ K and in ReB_2 with critical temperature varying from 4.5 to 6.3 K depending on boron concentration [8]. Kawano *et al* reported a new superconducting phase Re_7B_3 with $T_c = 3.3$ K [9].

Atoms of boron in MB_x compounds, (where M is the metal element) can form various structures. In MB_2 systems with AlB_2 structure B atoms form a two-dimensional honeycomb network (a well-known example is MgB_2). In the borides with higher metal content such as M_3B, M_2B or M_3B_2 the boron atoms are isolated or paired. Zig-zag chains can be found in MB type borides. Branched chains and double chains are present in $M_{11}B_8$ and M_3B_4 type borides, respectively.

Beside diborides, superconductivity has also been discovered in ternary compounds W–Re–X where X = B; C by Kawashima *et al* [10]. Examples are $W_7Re_{13}B$ and $W_7Re_{13}C$ with critical temperatures $T_c = 7.1$ K and 7.3 K, respectively. These materials were synthesized for the first time and their structural properties established almost thirty years ago by Kuz'ma [11] but never tested for the presence of superconductivity. The crystal structure of the $W_7Re_{13}B$ system is cubic, β-Mn-type, space group $P4_132$. Tungsten atoms occupy the 8(c) sites and rhenium atoms the 12(d) sites, while boron or carbon atoms occupy about one-quarter of the octahedral voids and thus stabilize the structure. Recently, the group of Kawashima also reported superconductivity in similar systems, namely in the compounds $Mo_7Re_{13}B$ with $T_c = 8.3$ K and $Mo_7Re_{13}C$ with $T_c = 8.1$ K [12].

One of the main obstacles to investigating the physical properties of these compounds is impurity phases [12, 13] or phases with different boron content as mentioned above. In the present work, the $W_7Re_{13}B$ sample was obtained using the inductive melting method which allowed us to avoid the formation of minority phases [14] and to obtain a pure superconducting phase. We report here on superconducting properties like critical and irreversibility fields, critical currents and high-pressure effects in the $W_7Re_{13}B$ intermetallic system. We also present theoretical calculations of the electronic structure of this compound.

2. Experimental details

The $W_7Re_{13}B$ intermetallic compound was synthesized by means of induction melting of the constituent elements in a water-cooled boat and under an argon atmosphere. Stoichiometric amounts of W, Re and B powders with a total mass of about 1 g were used for the melting. To ensure homogeneity, the ingot was inverted and remelted several times. This allowed us to obtain $W_7Re_{13}B$ polycrystalline samples of much better quality than the ones obtained by arc melting [10]. The experimental density of the $W_7Re_{13}B$ compound equal to 19.3 g cm^{-3} was very close to its theoretical value $\rho_{theor} = 19.47$ g cm^{-3}. The samples were next examined by powder x-ray diffraction using Co Kα radiation. The lattice constant, determined to be equal to 6.820 Å, was in good agreement with the earlier data reported by Kawashima *et al* [10]. The x-ray spectra did not show any minority phases, at least in amounts exceeding the sensitivity limit of the x-ray method equal to about 5% at volume. The x-ray photoemission spectra were recorded by means of a PHI 5700/660 Physical Electronics spectrometer. The radiation characterized by a photon energy equal to 1487.6 eV (Al Kα source) and a hemispherical mirror analyser with a resolution of about 0.3 eV was used for the measurements. The x-ray photoemission spectra were performed immediately after breaking the sample in a vacuum of 10^{-10} Torr.

The magnetometric measurements were performed by means of Oxford Instruments Ltd, a MagLab 2000 AC susceptometer/DC magnetometer and by a Quantum Design MPMS SQUID magnetometer. For measuring the upper critical field at high field range, a Quantum Design PPMS 14 T extraction magnetometer was used. For magnetic measurements versus temperature we applied zero-field-cooling (ZFC) and field-cooling (FC) procedures. The ZFC procedure consisted of cooling a sample to low temperature in the absence of a magnetic field. Next the field was applied and measurements were performed when warming the sample. During the FC procedure a sample was cooled in an applied magnetic field and measurements were simultaneously performed. The shape of the sample for magnetometric measurements was approximated by an ellipsoid of revolution with aspect ratio $\gamma = 1.33$, where $\gamma = l/2r$ and l, r are the lengths of the major and minor ellipsoid axes. This aspect ratio corresponds to the demagnetizing coefficient N equal to 0.266.

An easyLab Mcell 10 high pressure cell was fitted to the SQUID magnetometer to perform magnetometric measurements under high pressure. The cell enabled one to apply pressures of up to 1 GPa from room temperature down to the lowest temperature available in the magnetometer. The pressure inside the cell was practically invariant with temperature. However, below the solidification point of the pressure medium, i.e. around 200 K, the pressure should rather be regarded as quasi-hydrostatic than hydrostatic. For the high-pressure measurements, a part of the $W_7Re_{13}B$ ingot was ground into a fine powder and placed in a PTFE capsule together with a pure tin wire manometer (approximately 5 mm long and 0.25 mm in diameter). The capsule was next filled with Daphne oil, sealed and fitted into the high pressure cell. The cell was pressurized and then mounted on a standard SQUID magnetometer sample rod. The actual pressure in the cell was evaluated by measuring the pressure shift of the superconducting transition of tin. Here, the critical temperature of tin under pressure $T_c(P)$ was once again determined by means of magnetic moment measurements versus temperature $M(T)$ at an applied magnetic field of 1 mT. The pressure inside the cell was calculated using the parabolic function proposed by Smith [15]: $P = a[T_c(0) - T_c(P)]^2 + b[T_c(0) - T_c(P)]$, where P is in GPa T in K and the coefficients are equal to $a = 0.504\,1489$; $b = 1.781\,287$.

Because of the relatively strong magnetic background of the cell, the background was carefully subtracted from the total magnetic signal in the case of all high-pressure measurements. A bulk $W_7Re_{13}B$ sample was used for the measurements of lower and upper critical fields and critical current density at normal pressure. For the electric resistivity measurements a four-point contact method and Quantum Design PPMS 7 T bridge was used. The contacts were soldered directly to the sample using indium.

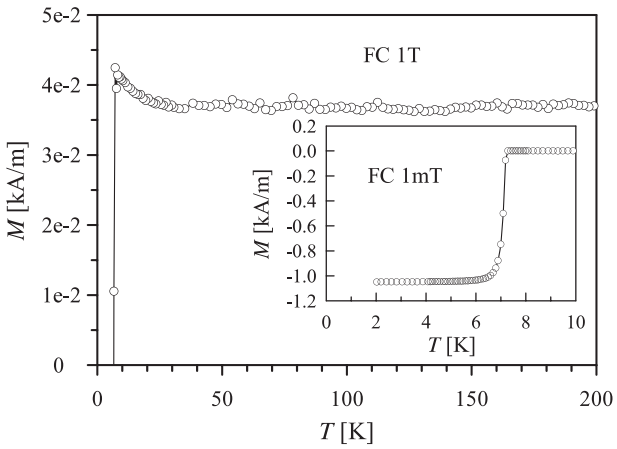

Figure 1. The dependence of FC magnetization on temperature $M(T)$ for the applied magnetic field equal to 1 T. The inset shows the superconducting transition for field cooling for the applied magnetic field equal to 1 mT.

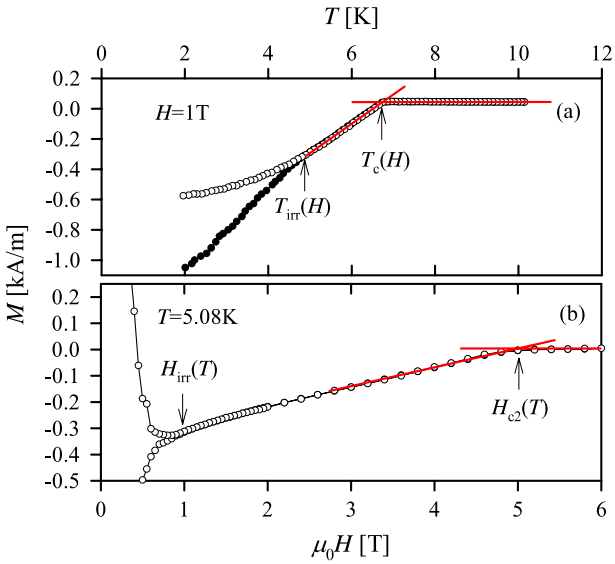

Figure 2. An example of variation in the magnetization of the $W_7Re_{13}B$ compound versus temperature $M(T)$ for the applied magnetic field equal to $\mu_0 H = 1$ T (a) and variation in the magnetization versus magnetic field $M(H)$ for the temperature equal to $T = 5.08$ K. The red lines show the criteria for $T_c(H)$ and $H_{c2}(T)$ whereas the arrows indicate $T_{irr}(H)$ and $H_{irr}(T)$.

3. Theory

The electronic structure was calculated for the ordered W_7Re_{14} compound characterized by the space group $P4_132$, no. 213 and lattice constant $a = 6.819$ Å. The unit cell consisted of 20 atoms. In the unit cell the W atoms are located at (0.061; 0.061; 0.061) and the Re atoms at (1/8; 0.206; 0.456) positions. To simulate the effects of pressure on the density of states (DOS), it was assumed that the positions of atoms and the lattice constant, a, vary within a few per cent. The full-potential local-orbital minimum-basis code (FPLO) was used and the band structure was calculated in the scalar-relativistic mode [16]. The numerical calculations were performed using the full-potential local-orbital minimum basis. The number of k points in the irreducible part of the Brillouin zone was 200. The parametrization of the exchange–correlation potential in the framework of the local spin density approximation was used in the form proposed by Perdew–Wang [17].

4. Results and discussion

Figure 1 in the main panel shows the FC magnetization $M(T)$ of the $W_7Re_{13}B$ compound versus temperature for the applied magnetic field equal to 1 T. In the inset there is shown the superconducting transition in $W_7Re_{13}B$ in a much lower magnetic field equal to 1 mT. At low temperature there dominates a strong diamagnetic signal due to the Meissner effect in the superconducting state. Above the transition to a normal state there also exist paramagnetic and Pauli contributions to the total magnetization. The paramagnetic contribution due to some paramagnetic impurities in the sample is significant up to about 50 K. Above this temperature there dominates a Pauli paramagnetic contribution. Taking into account also the diamagnetic term of free electrons, the total susceptibility at high temperature can be expressed as: $\chi = 2\mu_0\mu_B^2 D(E_F)/3$. In the above formula $D(E_F)$ is the density of states at the Fermi level and μ_B is the Bohr magneton. Additionally, we assume that the electron effective mass m^* is equal to the mass of free electron $m^* = m_e$. The density of states at the Fermi level calculated using the FPLO method is equal to $D(E_F) = 15.76$ [states eV^{-1}/fu] which corresponds to the theoretical susceptibility equal to $\chi_{SI} = 5.7 \times 10^{-5}$. The experimental value $\chi_{SI} = 4.6 \times 10^{-5}$ obtained for constant magnetization equals 37 A m^{-1} above 50 K and for the field 1 T is in reasonable agreement with theory if one takes into account that an error in $D(E_F)$ calculation is equal to about 20%.

The inset to figure 1 shows that for the low applied magnetic field the superconducting transition is very sharp and the magnetization reaches the lowest value within a few tenths of a kelvin below the transition. The width of the transition determined at 50% of diamagnetic signal is equal to 0.2 K and the critical temperature equals $T_c = 7.22 \pm 0.02$ K. This behaviour indicates bulk superconductivity and good quality of the sample. The superconducting transitions, however, become more gradual for higher magnetic fields, which makes difficult accurate measurements of the transition temperature, as it is shown in figure 2(a). This is why the critical temperatures corresponding to various magnetic fields $T_c(H)$ are determined from the intersection of the two straight lines fitting the linear regimes of $M(T)$ curves in normal and superconducting states, respectively. The linear regime in the normal state extends from the temperature above the superconducting transition up to 10 K. In this range of temperature and magnetization the paramagnetic contribution can be neglected. On the other hand, the linear regime in the superconducting state corresponds to the range from the superconducting transition down to the temperature where ZFC and FC magnetizations start to differ. This procedure allowed us to determine the relation of the mean-field upper critical field $H_{c2}(T)$ of the $W_7Re_{13}B$ compound on temperature as it is equivalent to the $T_c(H)$ dependence. The upper critical field $H_{c2}(T)$ can also be measured directly by cycling the magnetic field at constant

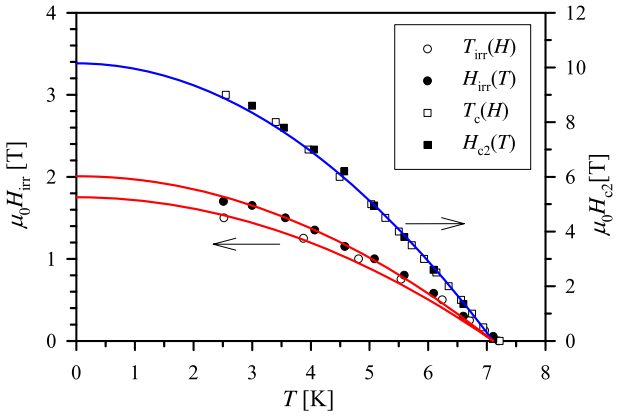

Figure 3. The critical temperature $T_c(H)$ versus magnetic field and the upper critical field $H_{c2}(T)$ dependence on temperature. Also shown are the irreversibility temperature $T_{irr}(H)$ and the irreversibility field $H_{irr}(T)$. The lines represent the best fits according to the two-fluid model.

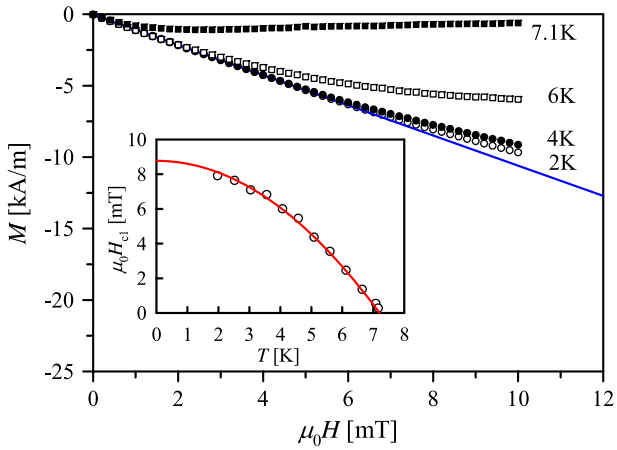

Figure 4. Magnetization of the $W_7Re_{13}B$ compound versus magnetic field $M(H)$ for different temperatures. Inset: the temperature dependence of the lower $H_{c1}(T)$ critical field. The line represents the two-fluid model fit to the experimental data.

temperature which is presented in figure 2(b). In this case, the upper critical field appears in the characteristic field where the diamagnetic signal vanishes and the magnetization changes its slope. The precise values of $H_{c2}(T)$ are determined here using once again the method of intersection of the two straight lines approximating the linear parts of $M(H)$ curves above and below the transition.

Beside the upper critical field, the plots of magnetization exhibit strong irreversibility below some characteristic temperature $T_{irr}(H)$ (figure 2(a)) or magnetic field $H_{irr}(T)$ (figure 2(b)). We define the irreversibility temperature $T_{irr}(H)$ as the temperature below which observable deviation is noted between ZFC and FC magnetization curves $M(T)$. By analogy, the irreversibility field $H_{irr}(T)$ is defined as the field below which there is observable difference between the $M(H)$ magnetization curves recorded for increasing and for decreasing magnetic fields. The results of all measurements i.e. $T_c(H)$, $H_{c2}(T)$, $T_{irr}(H)$ and $H_{irr}(T)$ are summarized in figure 3. It is evident that the $T_c(H)$ and $H_{c2}(T)$ data coincide very well and are located at the common curve in figure 3, whereas $T_{irr}(H)$ and $H_{irr}(T)$ are well separated from this curve.

A good fit of the experimental data is obtained using the Casimir–Gorter two-fluid model [18]; $H_{c2}(T) = H_{c2}(0)(1 - t^2)$, where $t = T/T_c$ is the reduced temperature. Because of the experimental error there is no need to use a more accurate fit according to BCS theory as it differs from the Casimir–Gorter model by a few per cent only, at the temperature near $T_c/2$. The upper critical field determined from the best fit is: $\mu_0 H_{c2}(0) = 10.15$ T. In the vicinity of the critical temperature, as can be expected, the data exhibit linear dependence with the slope $\mu_0\, dH_{c2}/dT = -2.38$ T K^{-1}. On the basis of the Werthamer–Helfand–Hohenberg formula [19]; $H_{c2}(0) \cong -0.69T_c(dH_{c2}/dT)$ for the value of dH_{c2}/dT as above and for $T_c = 7.22$ K, one obtains $\mu_0 H_{c2}(0) = 11.8$ T. This is above the value found from the fit, but still in good agreement with the value $\mu_0 H_{c2}(0) = 11.3$ T reported by Kawashima *et al* [10]. All the values are below the paramagnetic limit $\mu_0 H_p = 1.84\ T_c$ equal to 13.3 T. This suggests that the pair breaking mechanism due to Zeeman coupling is absent in the case of the $W_7Re_{13}B$ compound. The coherence length ξ calculated for $\mu_0 H_{c2} = 11.8$ T and from the relationship: $\mu_0 H_{c2} = \Phi_0/2\pi\xi^2$, where $\Phi_0 = 2 \times 10^{-15}$ Wb denotes the flux quantum is equal to 52 Å.

In contrast to the upper critical field measurements, the experimental results for irreversibility field $H_{irr}(T)$ and irreversibility temperature $T_{irr}(H)$ do not coincide—the irreversibility line determined from $H_{irr}(T)$ data is above that one found on the basis of $T_{irr}(H)$ data. This kind of discrepancy was also observed earlier by Suenaga *et al* in Nb_3Sn multifilamentary wires: however, no explanation was given in their report [20]. It seems that this disagreement can be due to the field inhomogeneity inside the magnet of the magnetometer, which is the most important obstacle to distinguish between very low but finite magnetic irreversibility and true reversible magnetization [21]. The influence of applied field inhomogeneity should be stronger for T_{irr} measurements where there is also some temperature gradient in the probe of the magnetometer during sweeping the temperature. Sample vibrations inside a space with a field and the temperature gradient should smooth any magnetic irreversibility and suppress the irreversibility line $T_{irr}(H)$ with respect to the $H_{irr}(T)$ one. Regardless of the discrepancies between $H_{irr}(T)$ and $T_{irr}(H)$ lines there is a surprisingly large temperature and field range of reversible flux motion in the H–T diagram for the $W_7Re_{13}B$ superconductor. The melting line, according to the melting theory [22], should reflect the superconducting–normal phase boundary $H_{c2}(T)$ over a wide range of temperatures except in the vicinity of the critical temperature where an irreversibility line exhibits positive curvature. Therefore the empirical formula $H_{irr}(T) = H_{irr}(0)(1 - t^2)$ identical to the expression for $H_{c2}(T)$ can be used to approximate the $H_{irr}(T)$ and $T_{irr}(H)$ data. The parameters of the best fit are: $\mu_0 H_{irr}(0) = 2$ and 1.75 T for the irreversibility line determined from H_{irr} and T_{irr} measurements, respectively.

Figure 4 presents magnetization dependence on low applied magnetic fields $M(H)$ for selected temperatures. From the slope of the linear part of the magnetization corrected for the demagnetizing effect it is possible to

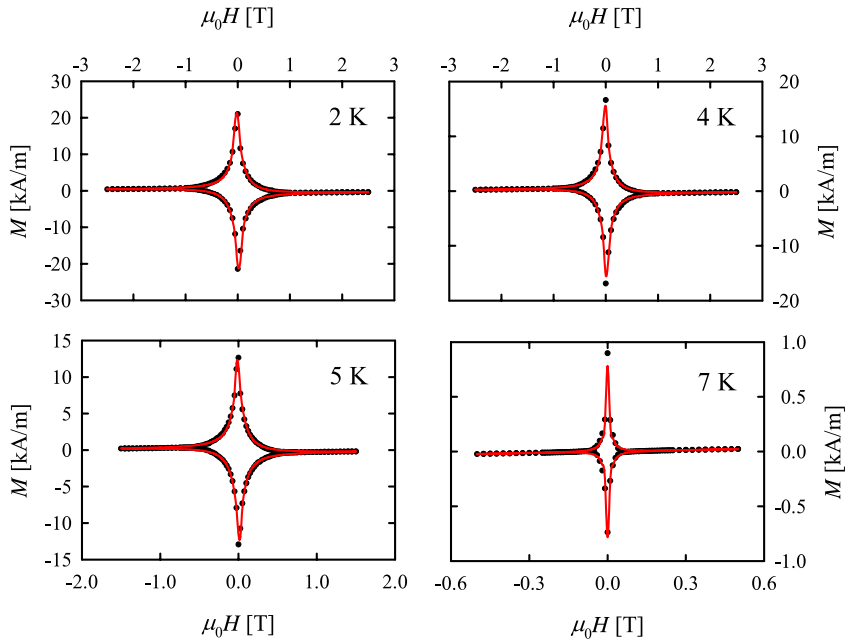

Figure 5. The set of magnetic hysteresis loops for the $W_7Re_{13}B$ compound for selected temperatures. The solid lines are fits according to the GCSM model.

estimate the fraction of the superconducting phase in the sample: $f_s = -(1 - N)M/H$. The calculated fraction is equal to 97%, which confirms bulk superconductivity in this compound. Also, using as a criterion the deviation of an initial part of the magnetization $M(H)$ from linearity one can find the values of the lower critical field at given temperatures, which is demonstrated in the inset to figure 4. This criterion allows an exact determination of the temperature dependence of the lower critical field $H_{c1}(T)$ in the case of 'classical' superconductors. It is invalid, however, for high-temperature superconductors. The behaviour of high-temperature superconductors is governed by surface barriers [23, 24] and very strong volume or surface pinning [25, 26], which hinder the penetration of the vortices into the sample. This leads to an overestimation of the lower critical field and also to its unusual upturn or positive curvature observed in the low-temperature range [27]. The temperature dependence of the lower critical field $H_{c1}(T)$ of the $W_7Re_{13}B$ compound corrected for a demagnetizing effect is presented in the inset to figure 4. Here, the flux pinning is not strong enough to affect the lower critical field and this latter exhibits usual behaviour with negative curvature. The data presented in the inset are once again fitted using the two-fluid model used previously with the parameters: $T_c = 7.2$ K and $\mu_0 H_{c1}(0) = 8.8$ mT. On the basis of the relation $\mu_0 H_{c1}(0) = (\Phi_0/4\pi\lambda^2)\ln(\lambda/\xi)$ this value of the lower critical field corresponds to the penetration depth equal to $\lambda = 2675$ Å.

The effect of flux pinning, important for the correct determination of the lower critical field, can be observed in figure 5 which presents the set of hysteresis loops recorded for various temperatures. In general, the hysteresis loops are very narrow and their irreversible behaviour vanishes very rapidly with applied magnetic field. Pinning forces acting on flux lines can be found from the critical state model [28]: $\boldsymbol{F}_p = -\boldsymbol{J}_c \times \boldsymbol{B}$, where the critical current $J_c(T, H)$ is related to the field gradient inside the sample $J_c(T, H) = \pm \mathrm{d}H/\mathrm{d}x$ and, in general, is temperature- and field-dependent. For most classical superconductors: $F_p = [H_{c2}(T)]^n f(b)$ where the first part describes temperature variation of the pinning force and $f(b)$ is a function only of reduced inductance $b = B/B_{c2}$ [29]. According to this, the critical current in zero magnetic field $J_c(0, T)$ should be proportional to the power of the upper critical field dependence on temperature; $J_c(0, T) \sim [H_{c2}(T)]^n$. There are many models describing the dependence of the critical current $J_c(H)$ on the magnetic field [30–37] but the most general is the generalized critical state model (GCSM) elaborated by Xu *et al* [38]. In GCSM the critical current is expressed as: $J_c(H, T) = J_c(0, T)/(1 + H/H_0)^m$, where $J_c(0, T)$ is the critical current density in the absence of the magnetic field and H_0 is a phenomenological coefficient. The critical current should vanish above the irreversibility line and therefore $J_c(H, T) = 0$ for $H > H_{irr}$. On the basis of the GCSM model and from the definition $M(H) = 1/V \int (H_i - H)\,\mathrm{d}V$, where V is the volume of the sample and H_i is the internal magnetic field, one can obtain the expressions for magnetization loops $M(H)$ and fit them to the data as is shown in figure 5.

The parameters $J_c(0, T)$ and H_0 of the best fits (see figure 6) are temperature-dependent, whereas the m coefficient is constant and equal to $m = 2.3$.

Even for the lowest temperatures available equal to 2 K and for zero applied magnetic field the critical current density is equal to 4.9 kA cm^{-2} only. The temperature dependence of the critical current in the absence of a magnetic field $J_c(0, T)$ can be well approximated by the expression: $J_c(0, t) = J_c(0, 0)(1 - t^2)$ which, for $n = 1$, is identical to the relation $J_c(0, T) \sim [H_{c2}(T)]^n$. The maximum value of the parameter H_0 is also small and equal to $\mu_0 H_0 = 0.175$ T. This allows us, in high field range, to reduce the GCSM formula to the power-law model: $J_c = J_c(0, T)/(H/H_0)^m$ proposed earlier by Irie

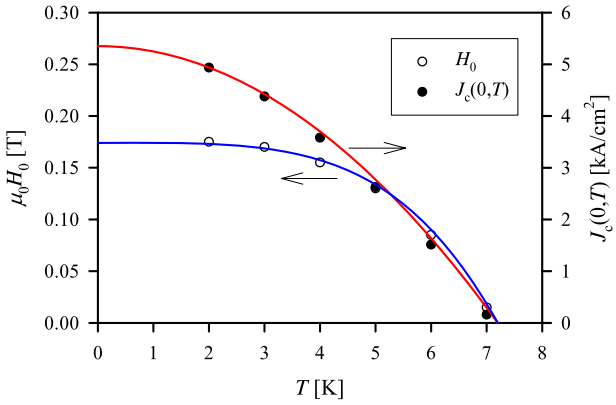

Figure 6. Critical current density at zero magnetic field $J_c(0, T)$ and the GCSM phenomenological coefficient H_0 versus temperature.

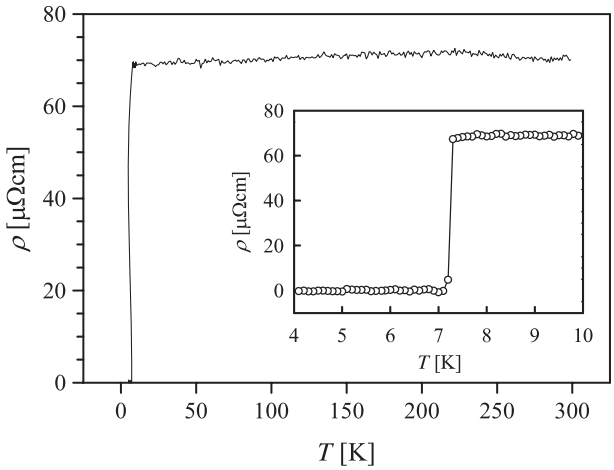

Figure 7. The temperature dependence of resistivity for the $W_7Re_{13}B$ compound. The inset shows the superconducting transition.

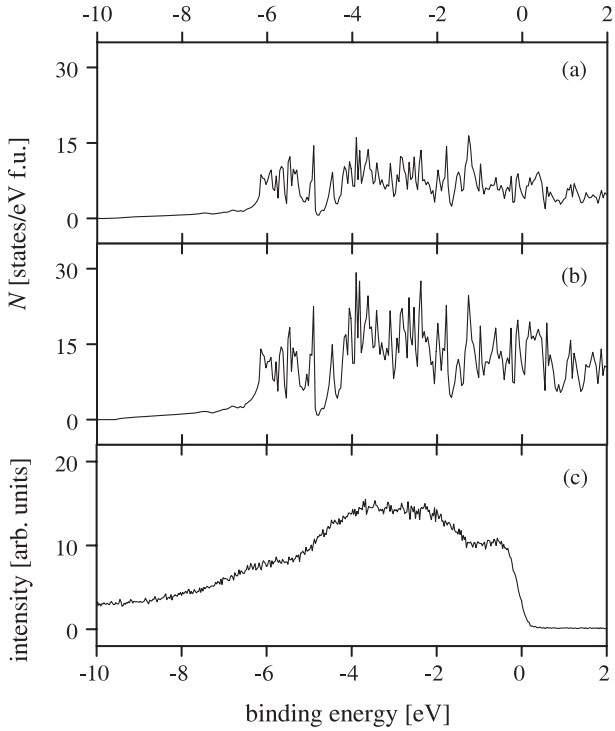

Figure 8. Theoretical calculations of the contributions to DOS from W (a) and Re (b). The XPS spectrum of the $W_7Re_{13}B$ compound is shown in (c).

et al [32]. Although there are suggestions that the parameter H_0 can be associated with the thermodynamic critical field H_c of some superconductors like Nb_3Sn and Nb–Zr [30] our results do not confirm this idea. Indeed, the temperature dependence of H_0 is much better fitted by the relation $H_0 \sim (1 - t^4)$ than the usual formula appropriate for critical fields, i.e. $H_0 \sim (1 - t^2)$.

Figure 7 presents the dependence of resistivity on temperature $\rho(T)$. The resistivity of the sample is almost constant in a wide temperature range, except for the superconducting transition. The onset of superconductivity, shown in the inset to figure 7 is very sharp and occurs at the temperature $T_c^{on} = 7.3$ K, slightly higher than that determined from magnetic measurements. The residual resistivity ratio defined as RRR $= \rho(T \approx T_c)/\rho$ ($T = 300$ K) is very close to 1. The room temperature resistivity ρ ($T = 300$ K) is equal to 70 $\mu\Omega$ cm. This value is about five times lower as compared to the sample obtained by arc melting. However, in spite of the much better quality of the present sample the overall temperature dependence of resistivity is very similar to that reported for the sample obtained by arc melting.

The relatively high value of resistivity as well as its negligible dependence on temperature can be explained in terms of boron excess deposited between superconducting grains. This explanation does not contradict the x-ray results indicating no trace of boron because, to make possible tunnelling of supercurrents, the layer of boron should be very thin and comparable to the coherence length ξ. In effect, the total amount of boron in the sample may be below the sensitivity limit of the x-ray method. Although the inductive melting substantially reduces the amount of unreacted boron between the grains, a trace of semiconducting characteristic of boron can be found also at the high temperature range where the resistivity initially increases as the temperature decreases.

In figure 8 there is shown the XPS spectrum of the $W_7Re_{13}B$ compound and the theoretical calculations of the contributions to the total density of states (DOS) from tungsten and rhenium. The main contributions to the binding energy comes from the W(5d) and Re(5d) states and the bands of the two elements are very similar. Substitution of W by Re does not change the total density of states. The theoretical results, i.e. equivalence of W and Re bands and equal contributions to DOS at the Fermi level contradict, however, the experimental data for the $Mo_7Re_{13}B$ compound [12]. The Mo substitution for W does not change much the critical temperature and other parameters of the superconducting state which should happen if the W band is involved in superconductivity. A similar conclusion can be obtained on the basis of high-pressure data because the pressure coefficient dT_c/dP for the $W_7Re_{13}B$ compound is close to that for Re—see the discussion below.

Figure 9 shows changes in the superconducting transition under pressure. One can notice that the critical temperatures are determined using as a criterion the intersection of the two straight lines fitting the two relevant regions of the $M(T)$

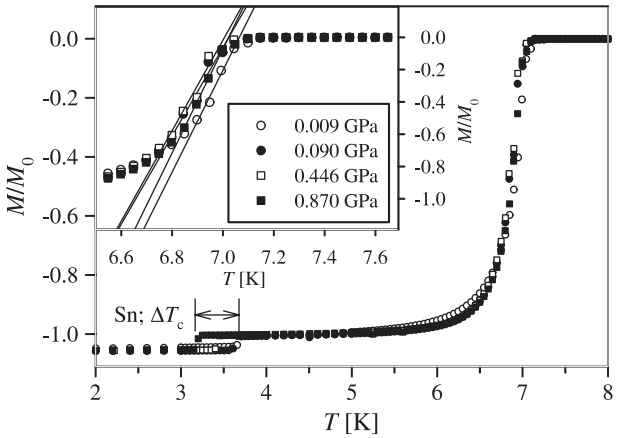

Figure 9. Normalized magnetization dependence on temperature for four different values of pressure. Notice the large pressure dependence of the superconducting tin transition at low temperature.

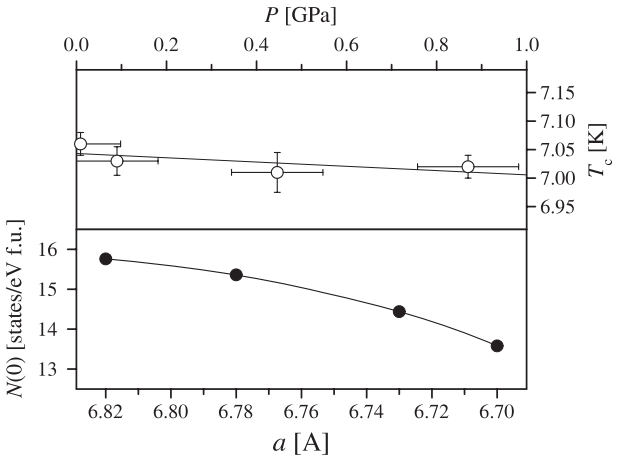

Figure 10. The pressure dependence of critical temperature for the $W_7Re_{13}B$ compound (upper panel) and the density of states at the Fermi level $N(0)$ with respect to lattice parameter a (lower panel).

curve. Due to the temperature gradient in the walls of the high-pressure cell, the $M(T)$ curves, and also the critical temperatures determined, are shifted to lower temperatures by 0.14 K with respect to previous measurements.

In figure 10 there is presented the dependence of critical temperature on pressure $T_c(P)$ and the density of states at the Fermi level with respect to lattice constant a.

From the experimental point of view, the decrease of the lattice constant is equivalent to the application of a pressure. Here, the DOS at the Fermi level decreases little as the pressure increases. It is evident that the influence of the pressure on the superconducting transition and on the critical temperature is very small in the applied pressure range. The pressure coefficient of the $W_7Re_{13}B$ compound is equal to -0.037 K GPa^{-1}, which is comparable with dT_c/dP coefficients for metallic Re equal to -0.017 ± 0.009 K GPa^{-1} reported by Bucher *et al* [39] or to -0.023 ± 0.01 K GPa^{-1} reported by Chu [40]. This can also indicate that the main contribution to superconductivity in the $W_7Re_{13}B$ compound is due to Re. According to the BCS relation $kT_c \sim \hbar\omega \exp[-1/N(0)V]$, where ω is a phonon frequency, $N(0)$ is the density of states near the Fermi level and V is the electron interaction, the critical temperature should decrease if the DOS decreases under pressure and if V is constant [41]. The relatively small changes in DOS at the Fermi level (less than 14% for a lattice contraction equal to 2%) correspond well with a small pressure effect in the $W_7Re_{13}B$ compound. A more trivial explanation is in terms of the low compressibility of this hard material. Thus one needs to apply higher pressures to induce more pronounced changes of the critical temperature.

5. Conclusions

We have synthesized and investigated the recently discovered $W_7Re_{13}B$ superconductor. Application of the method of inductive melting to the synthesis allowed us to obtain a pure superconducting phase exhibiting sharp transition and critical temperature equal to 7.22 K. The values of lower and upper critical fields of this superconductor are equal to 8.8 mT and 11.8 T, respectively. These correspond to the penetration depth and the coherence length equal to $\lambda = 2675$ Å, $\xi = 52$ Å and to the large Ginzburg–Landau parameter κ equal to 51. The value of the upper critical field is below the paramagnetic limit $\mu_0 H_p = 13.3$ T, which suggested that the pair breaking mechanism due to Zeeman coupling should be absent in this case. The superconductor exhibits type-II behaviour with a large part of the H–T diagram where the magnetic properties are reversible. The irreversibility field $\mu_0 H_{irr}(0)$ is equal to 2 T only and thus the irreversibility line is well separated from the upper critical field. The critical current density J_c at zero magnetic field and at temperature 2 K is about 4.9 kA cm^{-2}. The XPS spectrum together with numerical calculations confirm that the main contributions to the binding energy and to the density of states at the Fermi level came from the W(5d) and Re(5d) states. However, this contradicts the observation of superconductivity in the $Mo_7Re_{13}B$ compound and also with the pressure coefficient which is comparable to that of rhenium. The overall effect of pressure on superconducting properties is very small. The electrical resistivity of the $W_7Re_{13}B$ compound almost does not change with temperature and the residual resistivity ratio is very close to RRR ≈ 1. The negligible dependence of resistivity on temperature may be explained in terms of the boron excess deposited between superconducting grains.

Acknowledgment

BA acknowledges financial support from the EGIDE Foundation under the ECO-NET 10188YD project.

References

[1] Young D P, Goodrich R G, Adams P W, Chan J Y, Fronczek F R, Drymiotis F and Henry L L 2002 *Phys. Rev.* B **65** 180518
[2] Leyarovska L and Leyarovski E 1979 *J. Less-Common Met.* **67** 249–55
[3] Cooper A S, Corenzwit E, Longinotti L D, Matthias B T and Zachariasen W H 1970 *Proc. Natl Acad. Sci.* **67** 313–9

[4] Kaczorowski D, Zaleski A J, Żogał O J and Klamut J 2001 Incipient superconductivity in TaB_2 *Preprint* cond-mat/0103571

[5] Gasparov V A, Sidorov N S and Izver'kova I I 2006 *Phys. Rev.* B **73** 094510

[6] Gasparov V A, Sidorov N S, Izver'kova I and Kulakov M P 2001 *JETP Lett.* **73** 601–4

[7] Savitskii E M, Baron V V, Efimov Y V, Bychkova M I and Myzenkova L F 1973 *Superconducting Materials* (New York: Plenum)

[8] Strukova G K, Degtyareva V F, Shovkun D V, Zverev V N, Kiiko V M, Ionov A M and Chaika A N 2001 Superconductivity in the Re–B system *Preprint* cond-mat/0105293

[9] Kawano A, Mizuta Y, Takagiwa H, Muranaka T and Akimitsu J 2003 *J. Phys. Soc. Japan* **72** 1724–8

[10] Kawashima K, Kawano A, Muranaka T and Akimitsu J 2005 *J. Phys. Soc. Japan* **74** 700–4

[11] Kuz'ma Yu B, Lakh V I, Stadnyk B I and Voroshilov Y V 1968 *Sov. Metall. Ceram.* **6** 462

[12] Kawashima K, Kawano A, Muranaka T and Akimitsu J 2006 *Physica* B **378–380** 1118–9

[13] Kuz'ma Yu B, Lakh V I, Stadnyk B I and Voroshilov Y V 1968 *Test Methods and Properties of Materials* vol 7 (New York: Springer) p 462

[14] Kowalczyk A, Andrzejewski B, Jezierski A, Toliński T, Szlaferek A, Falkowski M and Chełkowska G 2006 *Acta Phys. Pol.* A **109** 597–600

[15] Smith T F, Chu C W and Maple M B 1969 *Cryogenics* **9** 53–6

[16] Koepernik K and Eschrig H 1999 *Phys. Rev.* B **59** 1743–57

[17] Perdew J P, Burke K and Ernzerhof M 1996 *Phys. Rev. Lett.* **77** 3865–8

[18] Gorter C J and Casimir H B G 1934 *Phys. Z.* **35** 963
Gorter C J and Casimir H B G 1934 *Z. Techn. Phys.* **15** 539

[19] Werthamer N R, Helfand E and Hohenberg P C 1966 *Phys. Rev.* **147** 295–302

[20] Suenaga M, Gosh A K, Xu Y and Welch D O 1991 *Phys. Rev. Lett.* **66** 1777–80

[21] Zheng D N, Ingle N J C and Campbell A M 2000 *Phys. Rev.* B **61** 15429–35

[22] Houghton A, Pelcovits R A and Sudbø A 1989 *Phys. Rev.* B **40** 6763–70

[23] Nideröst M, Frassanito R, Saalfrank M, Mota A C, Blatter G, Zavaritsky V N, Li T W and Kes P H 1998 *Phys. Rev. Lett.* **81** 3231–4

[24] Burlachkov L, Yeshurun Y, Konczykowski M and Holtzberg F 1992 *Phys. Rev.* B **45** 8193–6

[25] Hart H R and Swartz P S 1967 *Phys. Rev.* B **156** 403–11

[26] Pautrat A, Scola J, Goupil C, Simon Ch, Villard C, Domengès B, Simon Y, Guilpin C and Méchin L 2004 *Phys. Rev.* B **69** 224504–15

[27] Böhmer C, Brandstätter G and Weber H W 1997 *Supercond. Sci. Technol.* **10** A1–10 and references therein

[28] Bean C P 1962 *Phys. Rev. Lett.* **8** 250–3
Bean C P 1964 *Rev. Mod. Phys.* **36** 31–9

[29] Currie P D, Finlayson T R and Smith T F 1992 *J. Alloys Compounds* **183** 288–302

[30] Kim Y B, Hempstead C F and Strnad A R 1962 *Phys. Rev. Lett.* **9** 306–9

[31] Fietz W A, Beasley M R, Silcox J and Webb W W 1964 *Phys. Rev.* **136** A335–45

[32] Irie F and Yamafuji K 1967 *J. Phys. Soc. Japan* **23** 255–68

[33] Watson J H P 1968 *J. Appl. Phys.* **39** 3406–13

[34] Dersch H and Blatter G 1988 *Phys. Rev.* B **38** 11391–404

[35] LeBlanc D and LeBlanc M A R 1992 *Phys. Rev.* B **45** 5443–9

[36] Lera F, Navarro R, Rillo C, Angurel L A, Badia A and Bartolome J 1992 *J. Magn. Magn. Mater.* **104–107** 615–6

[37] Doyle T B, Doyle R A, Minkov D, Stepakin V N and Yakovets U P 1994 *Physica* C **233** 253–62

[38] Xu M, Shi D and Fox R F 1990 *Phys. Rev.* B **42** 10773–6

[39] Bucher E, Heiniger F, Muller J and Olsen J L 1965 *Low Temperature Physics LT9* Part A ed J G Daunt *et al* (New York: Plenum) p 616

[40] Chu C W, Smith T F and Gardner W E 1968 *Phys. Rev. Lett.* **20** 198–201

[41] Bardeen J, Cooper L N and Schrieffer J R 1957 *Phys. Rev.* **108** 1175–204